NASA Technical Paper 3028

June 1990

Loads Analysis and Testing of Flight Configuration Solid Rocket Motor Outer Boot Ring Segments

Rafiq Ahmed

NASA

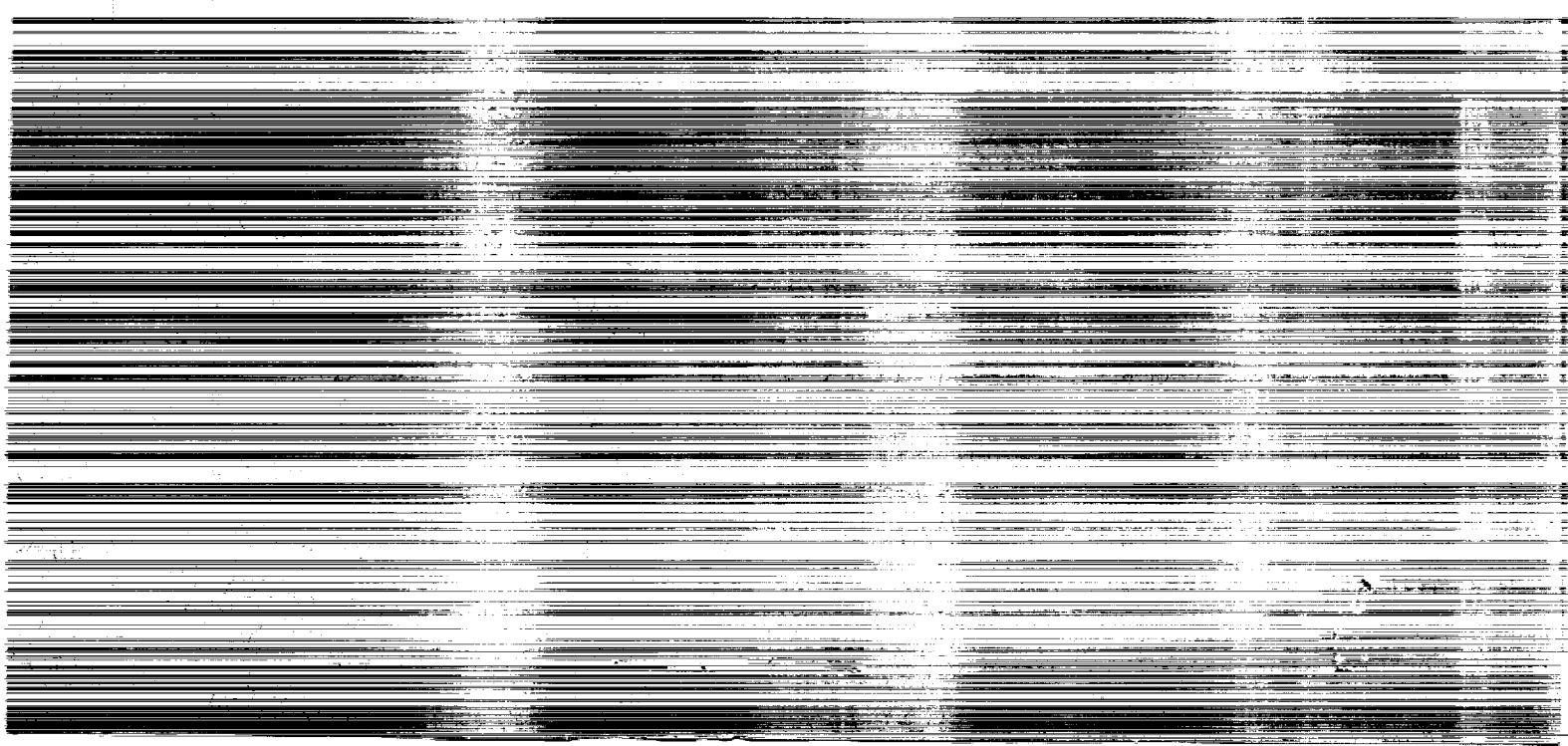

NASA Technical Paper 3028

1990

Loads Analysis and Testing of Flight Configuration Solid Rocket Motor Outer Boot Ring Segments

Rafiq Ahmed
George C. Marshall Space Flight Center
Marshall Space Flight Center, Alabama

National Aeronautics and Space Administration
Office of Management
Scientific and Technical Information Division

TABLE OF CONTENTS

LIST OF ILLUSTRATIONS

LIST OF ILLUSTRATIONS (Continued)

LIST OF ILLUSTRATIONS (Continued)

LIST OF ILLUSTRATIONS (Concluded)

LIST OF TABLES

TECHNICAL PAPER

LOADS ANALYSIS AND TESTING OF FLIGHT CONFIGURATION SOLID ROCKET MOTOR OUTER BOOT RING SEGMENTS

I. INTRODUCTION

After the Development Motor-9 (DM-9) involute carbon phenolic outer boot ring (OBR) failed during the test firing, NASA decided to commence post-Challenger shuttle flights with the DM-8 configuration "structural backup" OBR. This OBR configuration has proved satisfactory and is currently being used in the redesigned solid rocket motor (RSRM). In order to study the structural behavior and strength of this ring configuration, a series of four-point bending tests were initiated at MSFC using flat beams to closely simulate the ring's geometry. The radius of the boot ring is large enough to allow the use of flat beams (of the same cross section) to simulate a section of the boot ring.

A. Purpose

The objectives of the OBR load tests were as follows:

1. Assess the bending strength of the OBR segment.

2. Assess the load/stress versus strain relationships during bending for a linear elastic loading condition.

3. Determine what effect, if any, the position of the structural backup had on tension and compression load/stress versus strain relationships (i.e., backup side up versus backup side down).

4. Compare test results with analytical and finite element analyses accounting for anisotropy, ply angles, backup orientation, etc.

B. Summary

This report discusses the boot ring beam tests and presents the recorded test data in graphic form. The results of the two specimens used are compared with each other and with the analytical and finite element predictions. Assessments of the strength of the beams, the effect of the backup, stiffness, and agreement with predictions are given.

The tests were conducted between March 1, 1989, and May 15, 1989, at the MSFC Test Laboratory (ET52, now ED72). Strain gauges and electrodisplacement indicators (EDI's) were placed at various locations on each segment in order to record the load, strains, and displacements encountered. Analysis and data review were performed by the MSFC Structures and Dynamics Laboratory.

II. BOOT RING BEAM TESTS

The boot ring beam tests were conducted under the supervision of the MSFC Test Laboratory (ET52).

A. Test Specimens

Each of the two specimens was a 48-in long straight beam segment using the same construction as the current SRM OBR. This consists of a section of 35-degree carbon phenolic plies bonded to a "structural backup" section of 0-degree carbon phenolic plies. To simulate the OBR during mid-burn to end-of-burn conditions, a beam of rectangular cross section was designed with a 0.55-in thick 0-degree structural backup component bonded to a 1.20-in thick 35-degree section. The width of the beams was 6.5 in (Fig. 1).

B. Test Fixture

The test fixture consisted of a 50,000-lb load cell with a hydraulic actuator and all the appropriate hardware needed to load the specimen in four-point bending. The specimen was mounted with fixtures spaced 42-in apart and configured such that it could move in its longitudinal direction. Essential to a successful test was the proper application of the four-point bending loads to the segment. This was accomplished by using Teflon pads to distribute the load and minimize friction (thereby insuring a point load application) between load applicator and segment. A load point was applied 12-in from each mounting fixture (Fig.2).

C. Instrumentation

Each segment was instrumented by the Test Laboratory at MSFC with uniaxial and triaxial strain gauges. All gauges were placed at various positions in the middle of each specimen (Fig. 1). The uniaxial gauges measured tensile and compressive outer fiber strains as well as strains across the thickness. The triaxial gauges measured strains in the outer fiber and cross-width directions.

D. Procedure

Load was applied to the 48-in specimen via a single actuator and distributed to two loading pads, producing four-point bending. Two specimens were tested, each being loaded several times to half the expected ultimate strain (with the structural backup oriented both upward and downward) to simulate an elastic load case. The first segment was loaded three times elastically with the backup side up, three times elastically with the backup side down, and then loaded to failure with the structural backup oriented upward. The second specimen was also loaded elastically three times for each backup orientation, but was subsequently loaded to failure with the backup facing downward. Load, deflection, and strains were measured and recorded every 250 to 500 milliseconds during each of these tests. All tests were conducted at room temperature (approximately 70 °F).

E. Results

The deflections and strains at maximum load are shown in Table 1. The slopes of the elastic and "plastic" load versus longitudinal strain, load versus deflection, and load versus transverse strain plots are shown in Tables 2 and 3. Elastic and plastic slopes of these curves were computed using the linear regression routine in the Lotus 1-2-3 IBM-PC software. Figures 7 through 48 show the actual load versus deflection and load versus strain plots. Finally, the finite element model data are shown in Table 4.

III. MATHEMATICAL MODELS OF OBR BEAM SEGMENT

Hand analysis and finite element models were constructed to predict the behavior for the composite carbon phenolic material under the applied four-point bending load. Each is described below.

A. Hand Analysis

The hand analysis was based on treating the segment as a beam of constant cross section loaded in four-point bending with the following simplifying assumptions:

1. Since the elastic moduli in all three orthogonal directions are very similar, the carbon phenolic material was assumed to be isotropic. The material orientations were also ignored and simple beam theory was applied. Also ignored was the fact that the cross-ply material strength is significantly lower than the warp or fill strengths.

2. Shear coupling is assumed to be nonexistent (i.e., shear stresses are independent of normal stresses). The stress-strain relationships for normal tensors are independent from the shear stress-strain relationships.

3. Since the material is almost isotropic, no effective difference between the backup and 35-degree ply components of the beam is assumed.

4. Failure is conservatively assumed to occur as soon as the outermost fibers of the beam reach the nominal ultimate strength of the material.

5. The strains are assumed to be a linear function of distance from both tension and compression sides of the neutral axis. The stresses, on the other hand, are assumed to be linear as a function of distance on the compression side of the neutral axis and bilinear on the tension side of the neutral axis.

6. The deflection was calculated using the elastic deflection equation for four-point bending. This is not entirely accurate because the material undergoes plasticity before failure occurs; this method was used in the absence of relations describing the deflections of plastic beams.

Figure 1 shows the simply supported beam situation used to model the OBR beam test. Figures 3 and 4 show the shear and bending moment diagrams, respectively. Figure 5 exhibits the strain versus thickness and stress versus thickness diagrams assumed for the beam.

The calculation predicted the failure load to be 11,376 lb with a maximum deflection of 3.647 in. The details of how this analysis was derived are illustrated in the appendix.

B. Finite Element Analysis

The finite element representation of the beam was constructed using the FANTASTIC code developed by Failure Analysis Associates, Palo Alto, CA. FANTASTIC is designed for use in nozzle and nozzle component analysis and is well suited to model the 45-degree warp-fill bias commonly found in carbon and glass composite nozzle parts. The specimen was modeled in two dimensions and used a plane strain linear elastic solution scheme to simulate the elastic test runs. Since FANTASTIC's non-linear capability was not fully developed at the time of this writing, predictions of the plastic behavior of the beam could not be made. The model is shown in Figure 6.

The results of the two-dimensional finite element analysis are shown in Table 4, having given predictions for strain along the longitudinal axis of the beam and deflections perpendicular to the beam longitudinal axis.

IV. DISCUSSION

A. Failure Loads

This section compares the failure load for the backup-up specimen with that of the backup-down specimen. As shown in Table 1, the backup-up specimen and backup-down specimen exhibited approximately the same failure loads and deflections, although the backup-up specimen failed at a slightly higher load. This showed that the backup orientation had a little but noticeable effect on the final failure load of the beam. It should be noted that the backup comprised only about 31 percent of the beam's volume. The rest of the beam consisted of plies oriented at 35 degrees to the beam's longitudinal direction, which cause more cross-ply failures during loading. The cross-ply strength of carbon phenolics is much less than the warp and fill strengths.

B. Load Versus Strain and Deflection

As seen in metallic materials, the load versus strain and load versus deflection curves were linear in the elastic range with a decrease in slope as higher loads were reached. The decrease in slope happened over a small range of abscissa (strain or deflection) values, thus making the curves essentially bilinear. This is a valuable observation for hand and finite element analysis assumptions.

The elastic stiffnesses are essentially similar for both backup-up and backup-down beams. However, the bilinear transition point (the location on the curve where the material behavior changes markedly from elastic to plastic) is different between the two beams. This point occurs sooner on the backup-down specimen than on the backup-up specimen. This was attributed to the 0-degree plies being in tension on the backup-up specimen. Since these plies are oriented in the longitudinal direction (the direction

of the highest bending stresses), they will begin yielding at a higher load than the 35-degree plies of the backup-down section (which have a cross-ply stress component with respect to the longitudinal bending stress).

The agreement between the individual elastic runs for the two beams was essentially quite good, although some significant data scatter existed. All data was within 10 percent of each other; this is considered quite adequate for composite specimens. The average backup-up elastic bending modulus (load versus strain) for the first specimen was 1,357.0 kips and 1,381.0 kips for the second specimen. The backup-down values were 1,367.3 kips and 1,321.0 kips for the first and second specimens, respectively.

C. Comparison of Test and Hand Analysis

The failure loads for both ultimate tests ranged from 15,225 lb to 15,795 lb. This gives an average between the two specimens of 15,510 lb. The average deflection at failure was 3.84 in. The analysis predicted a failure load of 11,376 lb and deflection of 3.527 in, giving a percent difference of 26.7 percent for load and 8.2 percent for deflection. The predictions are conservative and could provide a good "rule of thumb" for analyzing carbon phenolic beams. It should be noted, however, that the analysis takes advantage of the similarity in values among the cross-ply, warp, and fill elastic moduli for the composite material. This similarity does not occur in most composites and would cause this hand analysis to break down when applied to them.

The difference between the test and this analysis can be primarily attributed to conservatively assuming that the beam fails as soon as the outer fibers reach their ultimate strain level. The beam actually maintains structural integrity even as the outer fibers fail, failing when a large portion of the internal fibers fail and create critical-size cracks. Using an isotropic material assumption does not take into account the material directionality that plays a big role in the material behavior.

D. Comparison of Test and Finite Element Analysis

As mentioned previouly, the FANTASTIC finite element code was used to perform the finite element analysis. This code is well suited to easily take into account varying ply angles and biases in SRM nozzle materials, with the ability to handle involute and tape wrap composites. However, the code could not at this writing perform a reliable nonlinear, plastic analysis.

This analysis predicted a strain of 1,830 microstrain and a deflection of 0.514 in at 3,000 lb load. At 6,000 lb, the strain and deflection were 3,660 microstrain and 1.028 in, respectively. The elastic slope for load versus deflection computed from these analyses was 5.837 kips/in (for both backup-up and backup-down cases). The load versus strain slopes from the analysis were 1,639.34 kips for backup-up and 1,511.34 kips for backup-down. The deflection stiffness from the model is essentially similar to the test results (within 4 percent for most data) whereas the model's strain stiffness is significantly larger than the test indicated (from 11 percent to 20 percent). Several phenomena may have caused this: flow of the phenolic resin that gives the composite its consistency, variation in material properties from published figures due to variations in processing or cure cycles, and/or creep underload. Refining the model's mesh density would yield more accurate results in the load-strain regime.

Note that, as expected, the model shows a larger stiffness for the backup-up case than for the backup-down case. This results from the added stiffness of the backup section in tension. Since the compressive strength is much greater in absolute value than the tensile strength (be it yield strength or ultimate strength), the higher modulus of the backup section results in a higher effective bending stiffness when it is in the tension position. The 35-degree nonbackup section has a lower effective stiffness due to the longitudinal ending stress being partially resisted in the low-modulus cross-ply direction. Such an effect is noticeable from the test data, but is much less than predicted by the analysis; this is also possibly due to creep or flow of the phenolic resin under load, which would cause more strain in the phenolic than expected. More tests should be made to more closely evaluate the viscoelastic behavior of carbon phenolic and other composite materials used in industry.

As finite element codes are further developed for use in the SRM nozzle industry, their nonlinear capability should improve. It would then be instructive to make nonlinear runs of these boot ring test configurations and compare them with the test results. Such phenomena as the bilinear transition region of the stress-strain curve (discussed earlier) could then be compared to the analysis.

Also important is that the material properties used in the finite element model are not well defined for composite materials. Differing processes in fabrication, layup, and cure cycles among batches of carbon phenolics can cause much greater scatter in material properties than is normal or acceptable for metallic materials. This would subsequently create inaccuracies between model and test data.

V. CONCLUSIONS

The bending strength of the beam is derived from the ultimate test load as described in the appendix and is found to be 14.47 kip-in/in with the backup side up and 13.95 kip-in/in with the backup side down.

In general, the finite element analysis and test results compared favorably in the linear elastic stress-strain region. Using a finer mesh would most likely have yielded even closer agreement, since coarse finite element models are generally too "stiff." Further development of the nonlinear composite analysis capability is needed to analyze the full loading spectrum, exhibiting the bilinear material behavior more accurately.

The analytical hand solution employed for these carbon phenolic beams gave conservative results and can be used to arrive at quick design solutions for carbon phenolic beams without creating a finite element model. However, it must be emphasized that this can only be used for carbon phenolic materials which have similar elastic moduli in the three orthogonal coordinate directions. Most other composite materials do not fit into this category.

As expected, the bending strength of the beam is greatest when the backup is oriented upward; the maximum strength in bending is realized when the material fibers are oriented parallel to the longitudinal stresses on the tension side. It is important to note that the tension side of the beam is the primary driver in the failure mechanism; the tensile strength is normally much lower than the compressive strength for a typical composite material.

The bilinear transition point is a quantity unique to the bending of composite materials in that it depends on the orientation of the backup. This transition between the elastic and plastic portion of the load-strain and load-deflection curves occurs at a higher strain for the backup-up case than with the backup-down. This can be important when deciding how to orient the beam during the design process.

Further investigation of tension, compression, bending, buckling, viscoelasticity and other physical processes are necessary to better understand composite material behavior and to develop better design criteria for composite structures. The series of tests described in this report only utilized two beam specimens. More specimens need to be fabricated and tested to gather more and different types of data. The scope of a complete test program would include all of the aforementioned physical phenomena.

BIBLIOGRAPHY

1. Beer, F., and Johnston, E.: "Mechanics of Materials." McGraw-Hill, 1981.

2. Timoshenko, S., and Goodier, J.: "Theory of Elasticity." McGraw-Hill, 1951.

3. Dally, J., and Riley, W.: "Experimental Stress Analysis." McGraw-Hill, 1965.

4. Bolieau, D.J., et al: "RSRM Nozzle Stress Report." TWR-16975, Morton-Thiokol Wasatch Division, November 25, 1987.

5. Rebello, C.J., et al: "Space Shuttle RSRM Nozzle Materials Data Book." TWR-15995, Morton-Thiokol Wasatch Division, November 25, 1987.

6. Gutierrez-Lemini, D., et al: "RSRM Structural Material Properties Data Book." TWR-18011, Morton-Thiokol Wasatch Operations, April, 1988.

7. "FANTASTIC/FAST Structural Analysis Module, Version 1.3, User's Manual." Failure Analysis Associates, June 1989.

8. "FANTASTIC/PATRAN Translators, Version 1.3, User's Manual." Failure Analysis Associates, June 1989.

APPENDIX

DERIVATION OF FAILURE LOAD FOR DM8 OUTER BOOT RING SPECIMENS IN FOUR-POINT BENDING

The following assumptions were made in order to analyze this situation:

1. The carbon phenolic material is assumed to be isotropic at room temperature since all three elastic moduli are approximately the same.

2. Shear coupling terms are neglected (i.e., shear stresses are independent of the normal stresses).

3. There is no effective difference between backup and nonbackup parts of beam.

4. Failure is assumed to occur as soon as outer fiber reaches ultimate stress.

The following stress and strain profiles are exhibited through the thickness of the beam when looking at a longitudinal cross section of the beam:

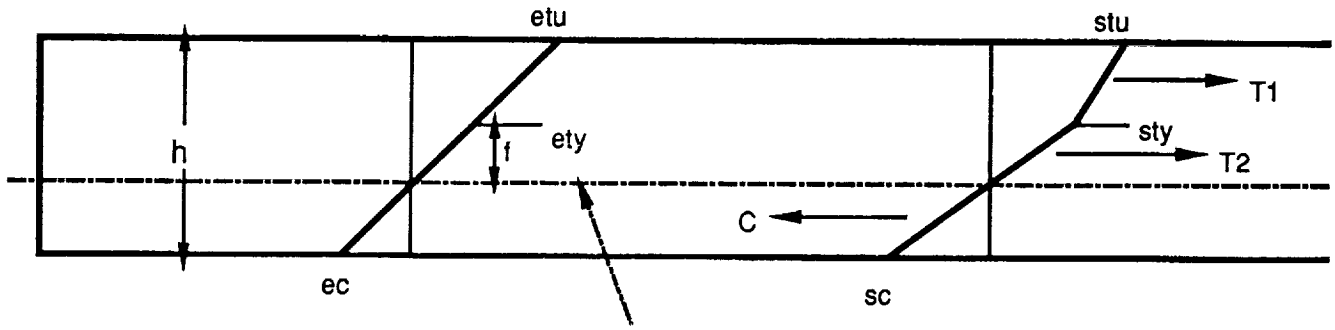

Note that a linear strain distribution is assumed as a function of distance from either side of the neutral axis of the beam. The tension stress-strain curve is assumed bilinear and the compression curve is assumed linear with the ultimate compression strength having a higher absolute value than the tension yield strength. These assumptions agree well with previous experimental data. Therefore, the neutral axis of the beam shifts toward the compression side of the beam. The beam is assumed to have the same material properties all through its thickness. The following material properties are used:

s_{tu} = ultimate tensile strength = 16,000 psi

s_{ty} = yield tensile stress = 8,000 psi

e_{tu} = ultimate tensile strain = 0.012

e_{ty} = yield tensile strain = 0.003

s_{cu} = ultimate compressive stress = 42,600 psi

e_{cu} = ultimate compressive strain = 0.0168

h = height = 1.75 in

f = location in beam thickness direction where fibers first start to yield

j = neutral axis location

1. First, the location of the neutral axis, j, is found using similar triangles:

$$f/e_{ty} = (h-j)/e_{tu} = j/e_c \quad .$$

Rearranging this yields,

$$f = (e_{ty}/e_{tu})\,(h-j) \quad .$$

Integrating the stress-strain curve gives:

$$T1 = s_{ty}\,(f/2) = (s_{ty}/2)\,(e_{ty}/e_{tu})\,(h-j)$$

$$T2 = [(s_{tu}+s_{ty})/2]\,(h-j-f) = [(s_{ty}+s_{tu})/2]\,(h-j)\,(1-e_{ty}/e_{tu})$$

$$C = (s_c/2)j = (s_{cu}/e_{cu})\,[e_{tu}\,j/(h-j)]\,(j/2) \quad .$$

Noting that T1 + T2 – C = 0 by equilibrium and substituting the appropriate values given above into these equations gives the following:

$$j^2 + 6.712j - 5.873 = 0 \quad .$$

Solving the quadratic equation gives j = 0.784 in.

Solving for T1, T2, and C yields:

T1 = 966.47 lb/in

$T2 = 8{,}697.6$ lb/in

$C = 9{,}666.82$ lb/in .

2. Now the moments are summed about the neutral axis to obtain the total bending moment acting on the beam:

$$m = -C(j/3) = T1(j+0.666f) + T2[j+f+(h-j-f)/2]$$

where

$$f = e_{ty}/e_{tu}(h-j) = 0.25\ (1.75-0.787) = 0.242 \text{ in}$$

$h-j-f = 0.725$ in .

Substituting the given values into this equation yields $m = 10{,}774.73$ lb-in/in

$M = mb = 70{,}574.47$ lb-in since $b = 6.55$ in = width of the beam.

3. Now the four-point bending relation that equates force with the total moment is used to determine the load at each pad:

$$M = (P/2)a$$

where a = the distance from a beam support to the nearest load pad = 12 in

$P/2 = M/12 = 5{,}881.2$ lb .

The total load is $P = 11{,}762.4$ lb predicted to cause failure in the outermost tension fibers.

4. To calculate the deflection, the four-point bending deflection equation is used as an approximation (this assumes that the beam is elastic at failure):

$$y_{max} = (Pa/24EI)\ (3L^2 - 4a^2) = 3.647 \text{ in} ,$$

where

$$a = 12 \text{ in} , \quad L = 42 \text{ in} , \quad E = 2.6 \text{ Msi} , \quad I = 2.925 \text{ in}^4 .$$

To summarize, the predicted failure load is 11,762.4 lb with a deflection at failure of 3.647 in.

TABLE 1. LOAD, DEFLECTION, STRAIN AT MAXIMUM LOAD DURING ULTIMATE TESTS

(LOAD IN LBS, DEFLECTION IN INCHES, STRAIN IN MICROSTRAIN)

Test #	L1001	D1	D2	D3	1T1001	2T1001	3T1001	1T1002
1	15795	3.89	0.98	0.39	18148.5	6854.9	-5833.5	-13374.3
2	15225	3.79	0.64	0.62	19666.6	7969.55	-5894.5	-13342.3

Test #	2T1002	3T1002	S1001	S1002	S1003	S1004
1	-5039.9	4346.1	18899.1	-12655.6	20210.3	-12983.7
2	-4825.3	4519	-12954.1	18863.6	-13088.5	19428.2

TABLE 2. ELASTIC SLOPES OF LOAD VERSUS STRAIN, DEFLECTION CURVES

Test #	Kips Load/Max. Tens. Strain	Kips/in Load/Defl.	Kips Load/Trans. Strain
Backup Up #1	1423	6.26	-4810
Backup Up #2	1346	6.08	-4610
Backup Up #3	1345	6.08	-4610
Backup Dn #1	1355	5.91	-4680
Backup Dn #2	1374	5.97	-4810
Backup Dn #3	1373	5.97	-4810
Backup Up Ult.	1314	5.99	-4550
Backup Up #1	1392	6.06	-4480
Backup Up #2	1377	6.08	-4430
Backup Up #3	1374	6.08	-4410
Backup Dn #1	1307	5.87	-4330
Backup Dn #2	1335	5.96	-4460
Backup Dn #3	1336	5.96	-4460
Backup Dn Ult.	1306	5.89	-4390

TABLE 3. PLASTIC SLOPES OF LOAD VERSUS STRAIN, DEFLECTION CURVES

Test #	Kips Load/Max.Tens. Strain	Kips/in Load/Defl.	Kips Load/Trans. Strain
Spec.#1 Ult. (backup up)	462	2.68	-1460
Spec.#2 Ult. (backup dn)	506	3.01	-1570

TABLE 4. LOAD AND DEFLECTION FINITE ELEMENT MODEL PREDICTIONS

Test	Kips Load	in Deflection	microstrain Max. Long. Tension Strain
Backup Up	0	0	0
	3	0.514	1830
	6	1.028	3660
	9	1.542	5500
	12	2.056	7330
	15	2.570	9160
Backup Down	0	0	0
	3	0.514	1990
	6	1.028	3970
	9	1.542	5960
	12	2.056	7950
	15	2.570	9930

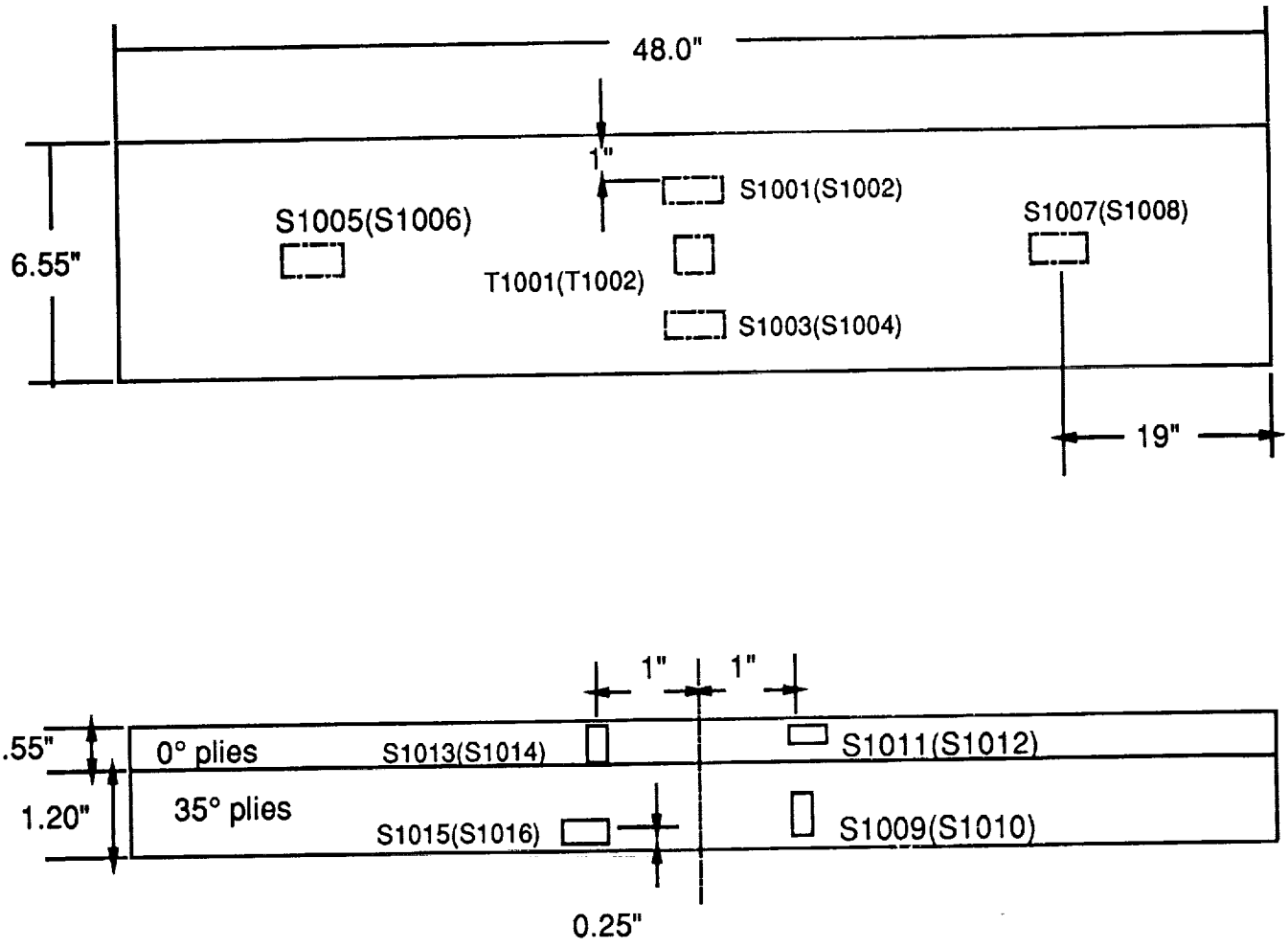

NOTE: Label numbers in parantheses represent gauges on opposite surface

Figure 1. MSFC fabricated OBR beam segment configuration.

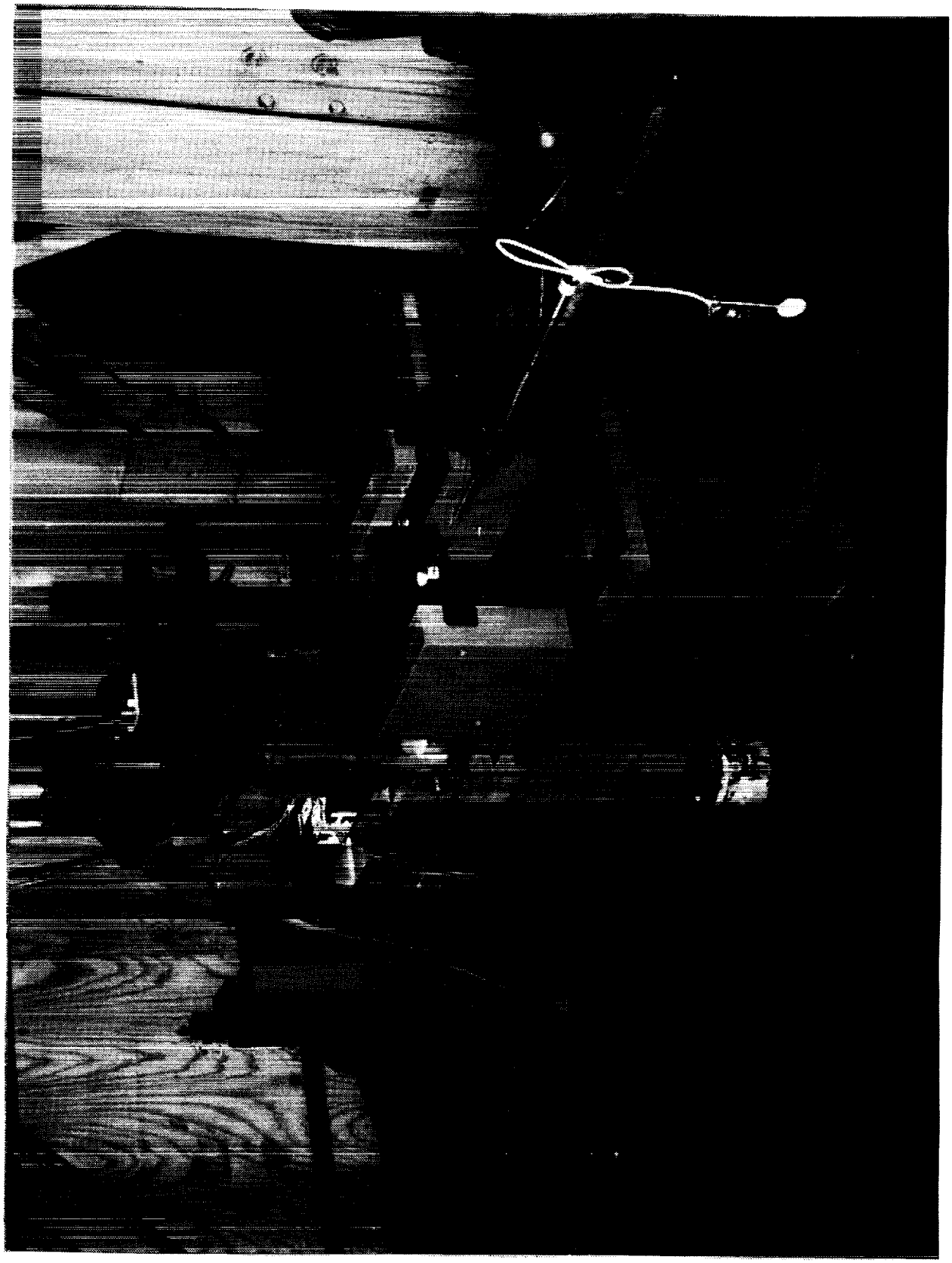

Figure 2. Boot ring beam test setup.

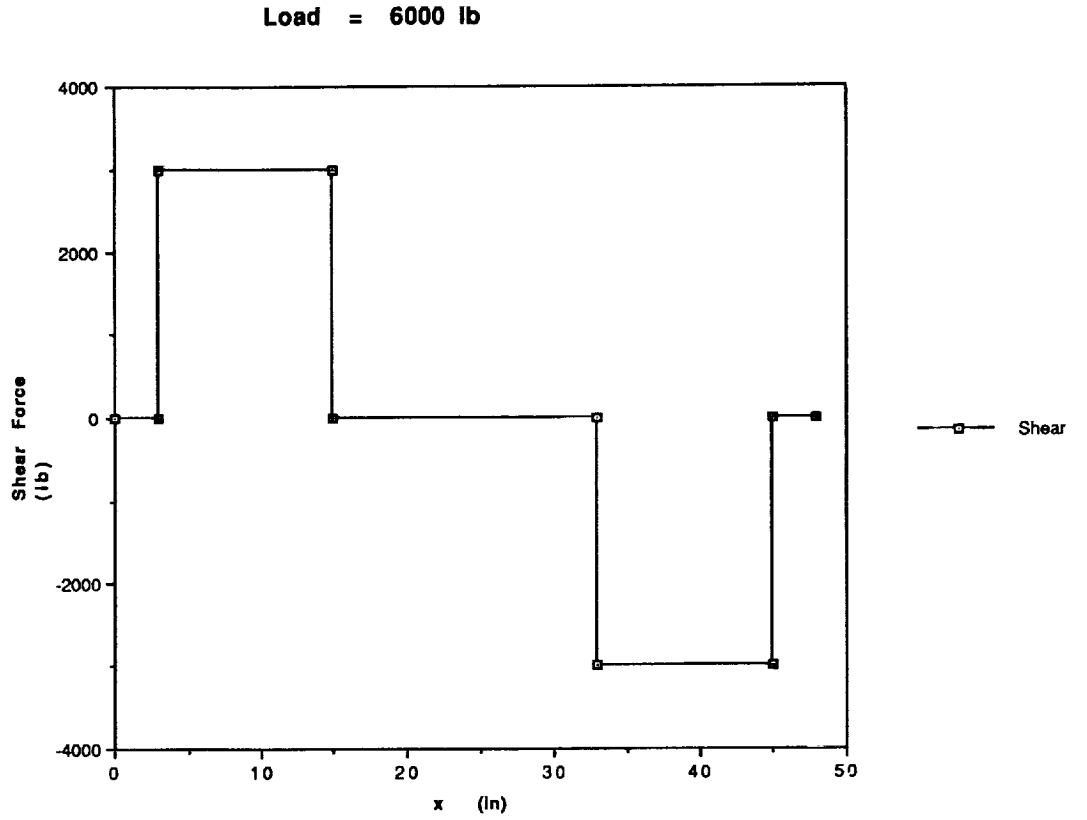

Figure 3. Boot ring beam shear diagram.

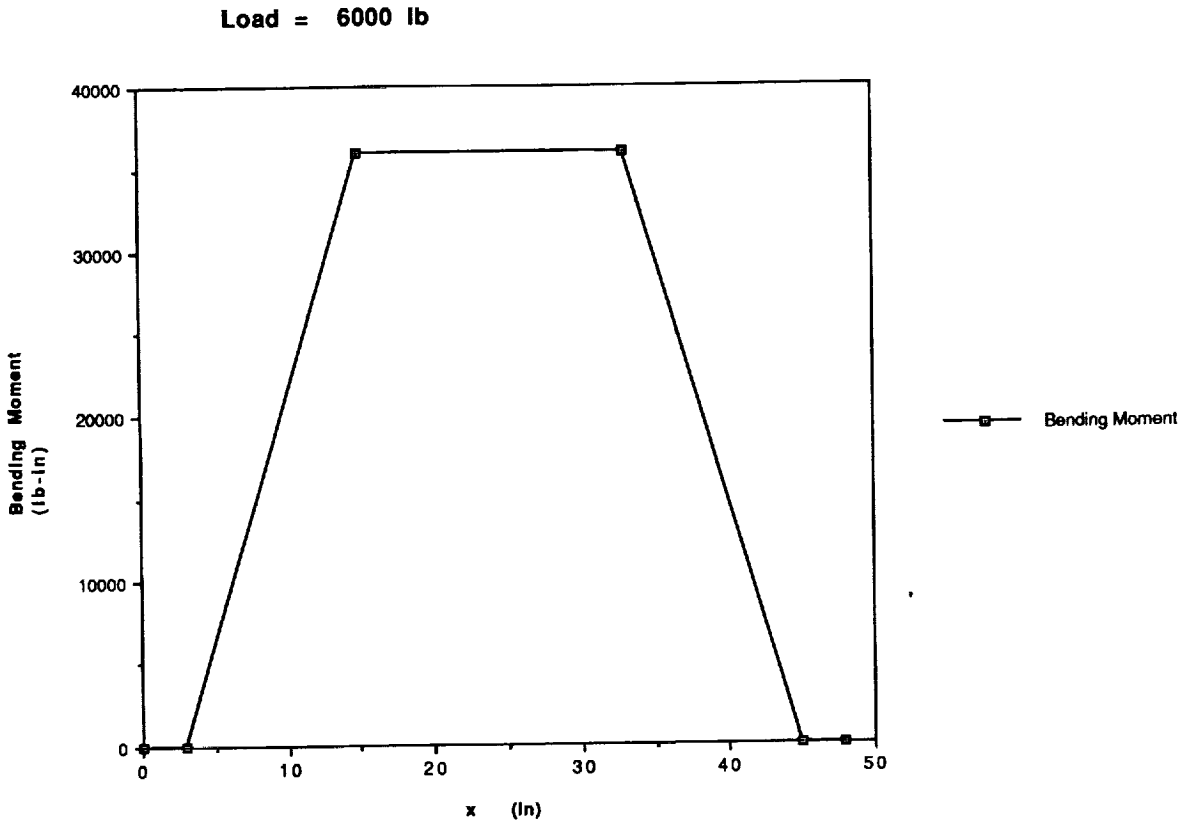

Figure 4. Boot ring beam bending moment diagram.

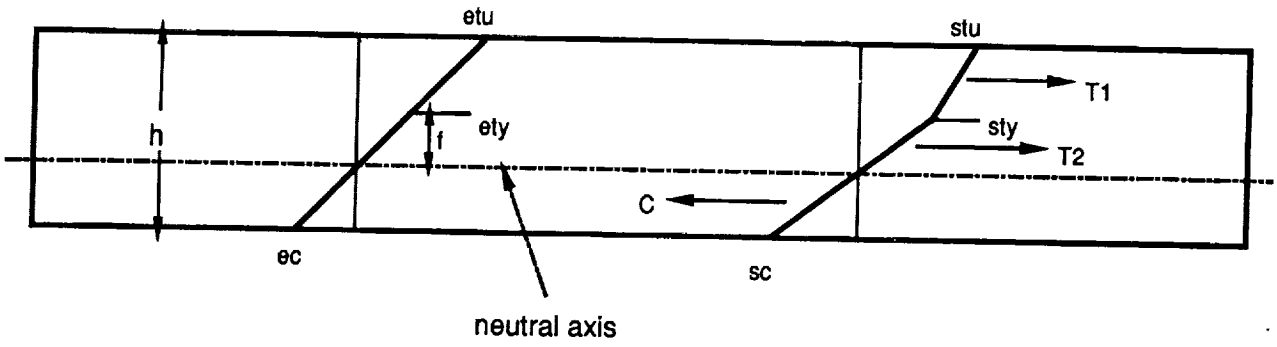

stu = ultimate tensile strength = 16,000 psi
sty = yield tensile stress = 8,000 psi
etu = ultimate tensile strain = 0.012
ety = yield tensile strain = 0.003
scu = ultimate compressive stress = 42,600 psi
ecu = ultimate compressive strain = 0.0168
h = height = 1.70 in
f = location in beam thickness direction where fibers first start to yield
j = neutral axis location

Figure 5. OBR beam stress-strain profiles through thickness.

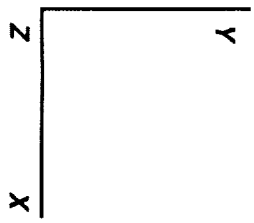

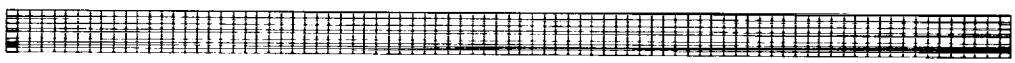

Figure 6. Finite element representation of boot ring beam.

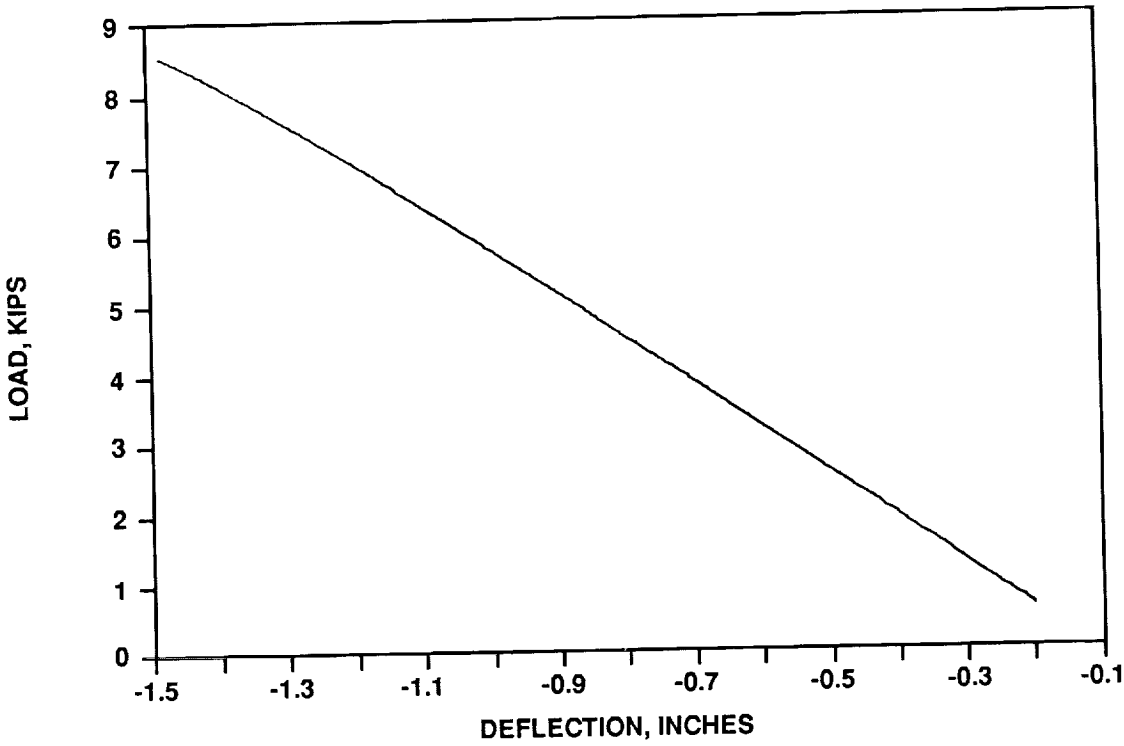

Figure 7. Boot ring beam test No. 1, backup-up 3/9/89, load versus deflection, specimen No. 1.

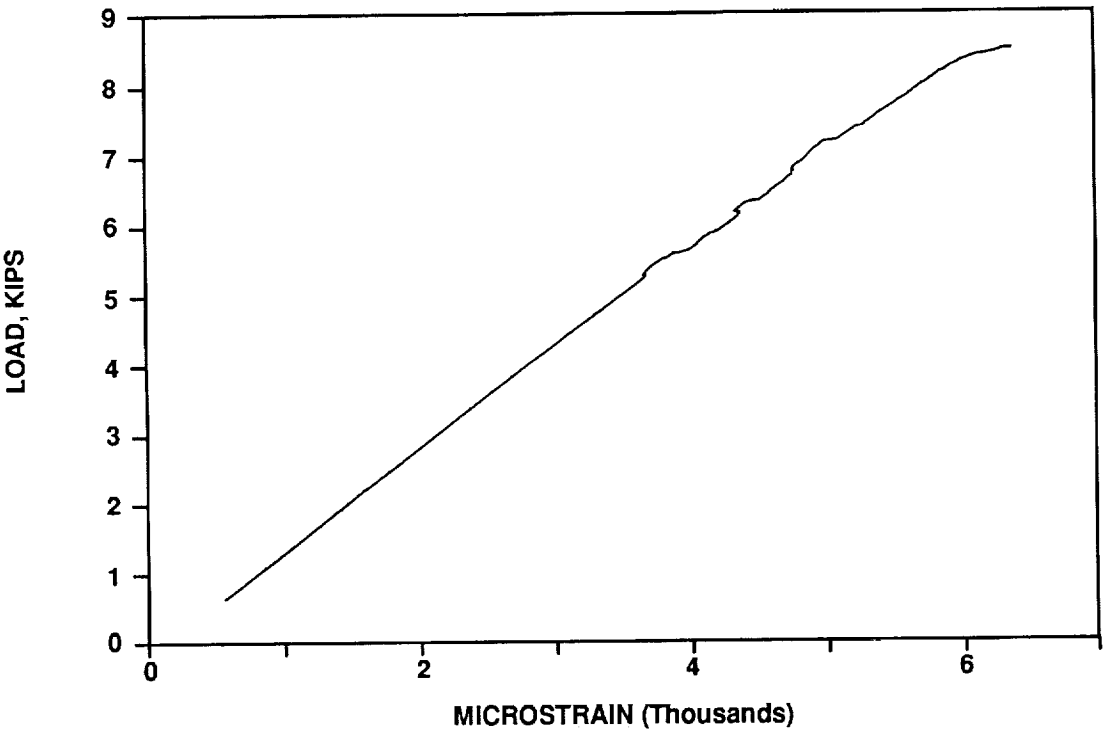

Figure 8. Boot ring beam test No. 1, backup-up 3/9/89, load versus maximum tension strain, specimen No. 1.

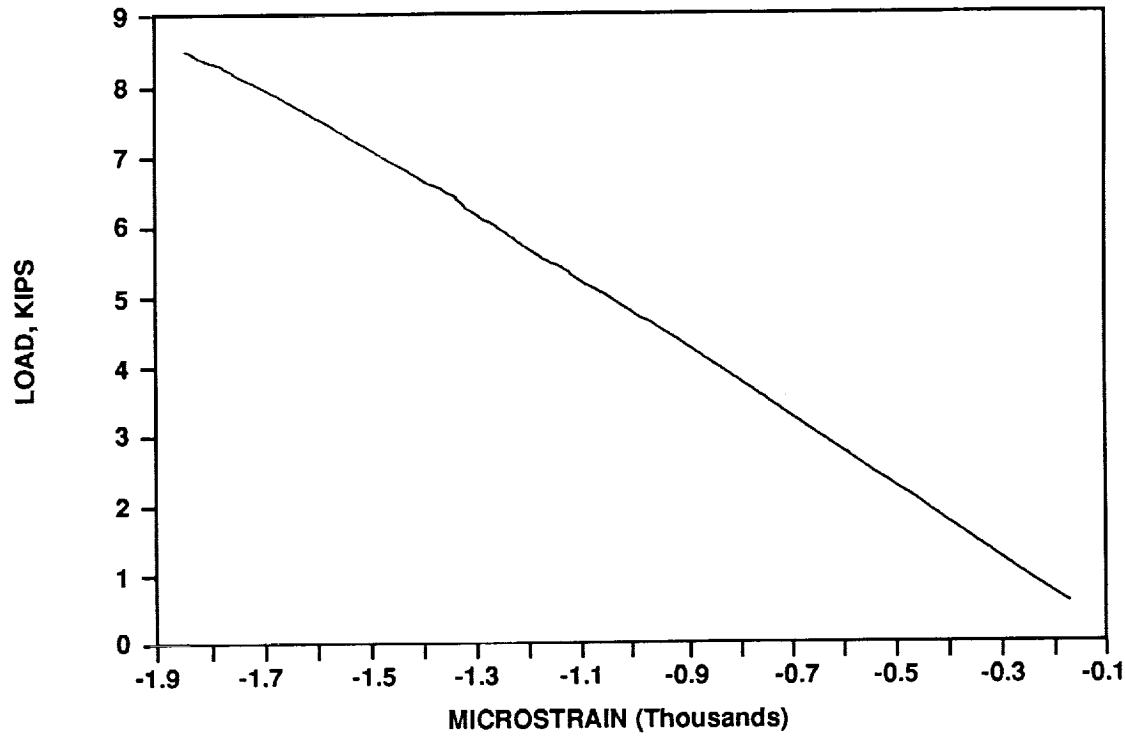

Figure 9. Boot ring beam test No. 1, backup-up 3/9/89, load versus maximum transverse strain, specimen No. 1.

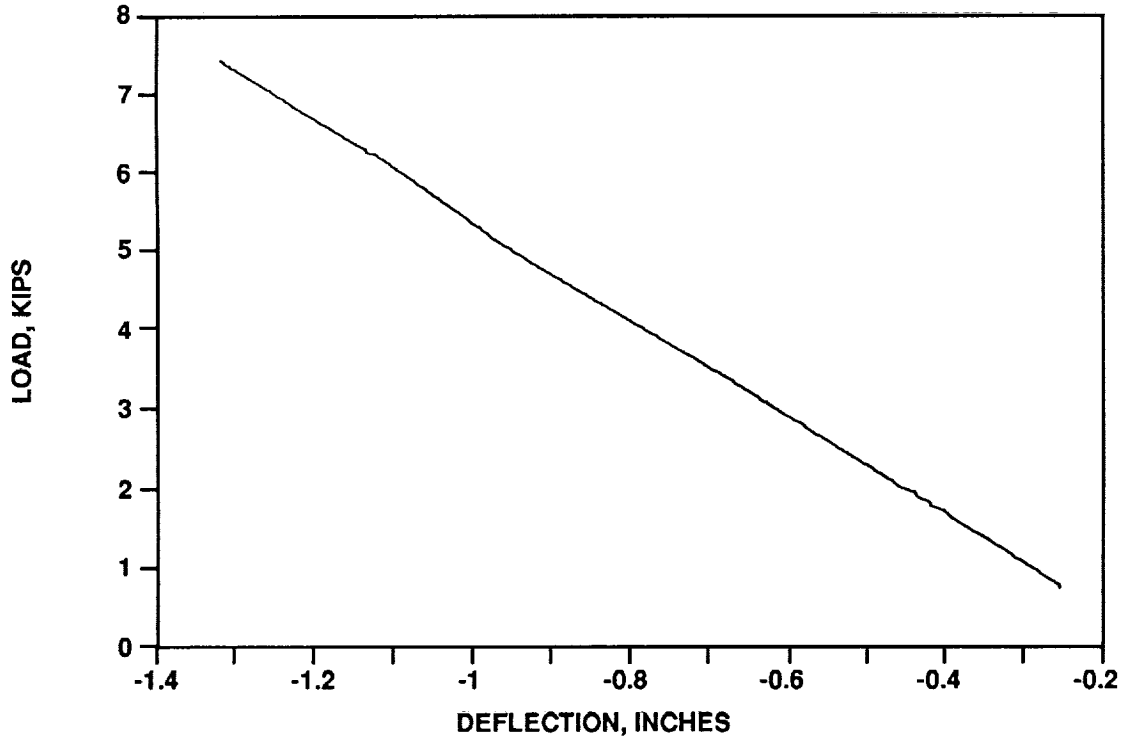

Figure 10. Boot ring beam test No. 2, backup-up 3/9/89, load versus deflection, specimen No. 1.

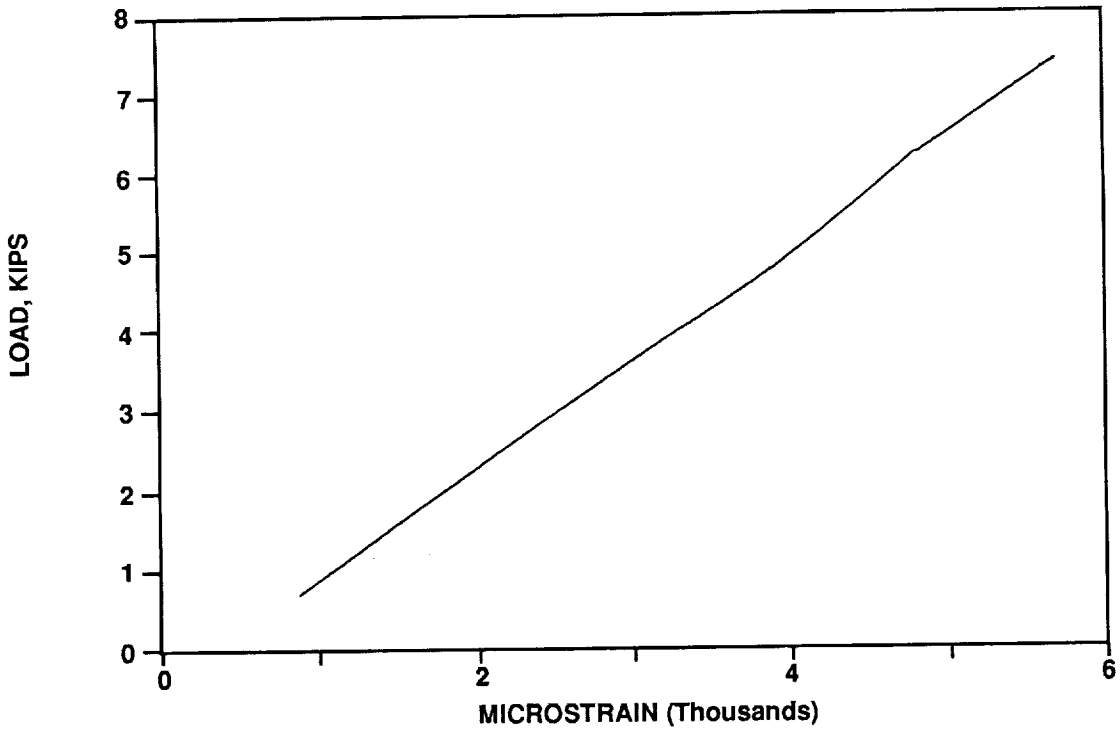

Figure 11. Boot ring beam test No. 2, backup-up 3/9/89, load versus maximum tension strain, specimen No. 1.

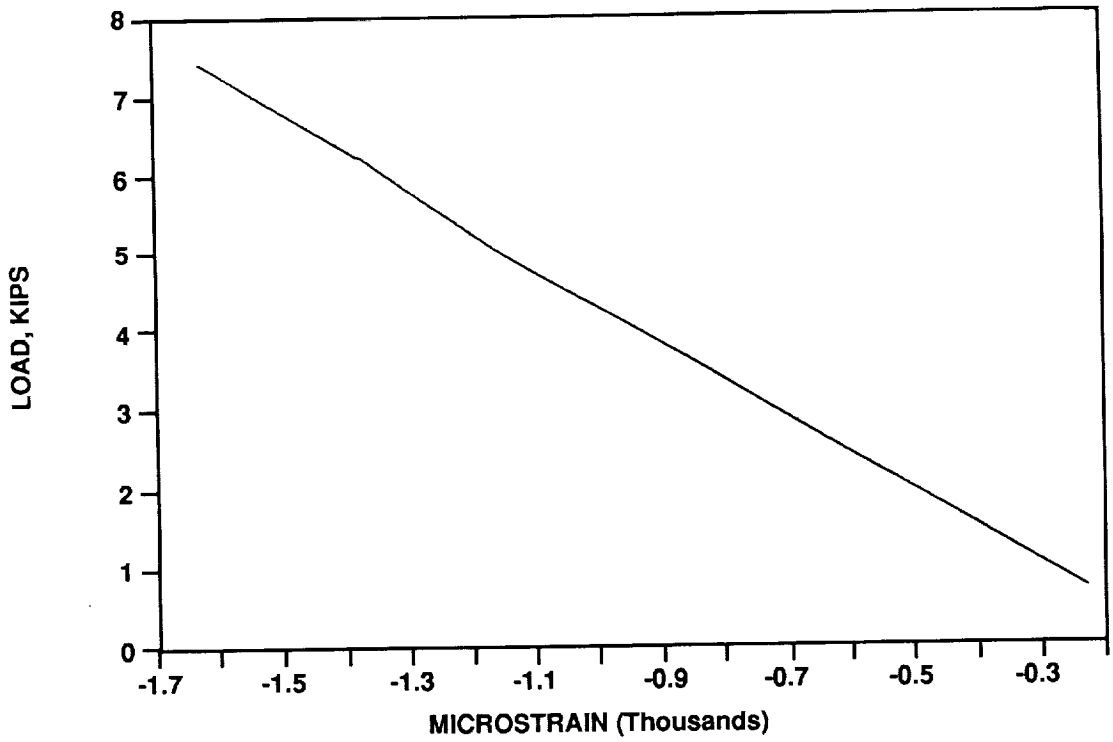

Figure 12. Boot ring beam test No. 2, backup-up 3/9/89, load versus maximum transverse strain, specimen No. 1.

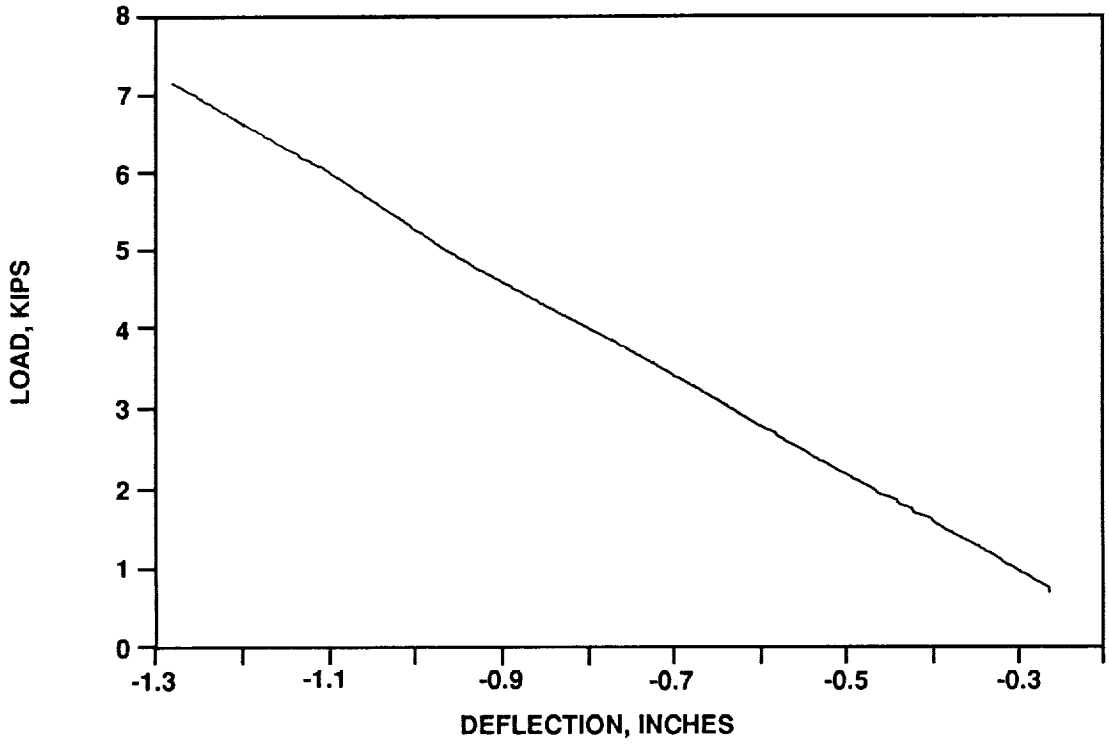

Figure 13. Boot ring beam test No. 3, backup-up 3/9/89, load versus deflection, specimen No. 1.

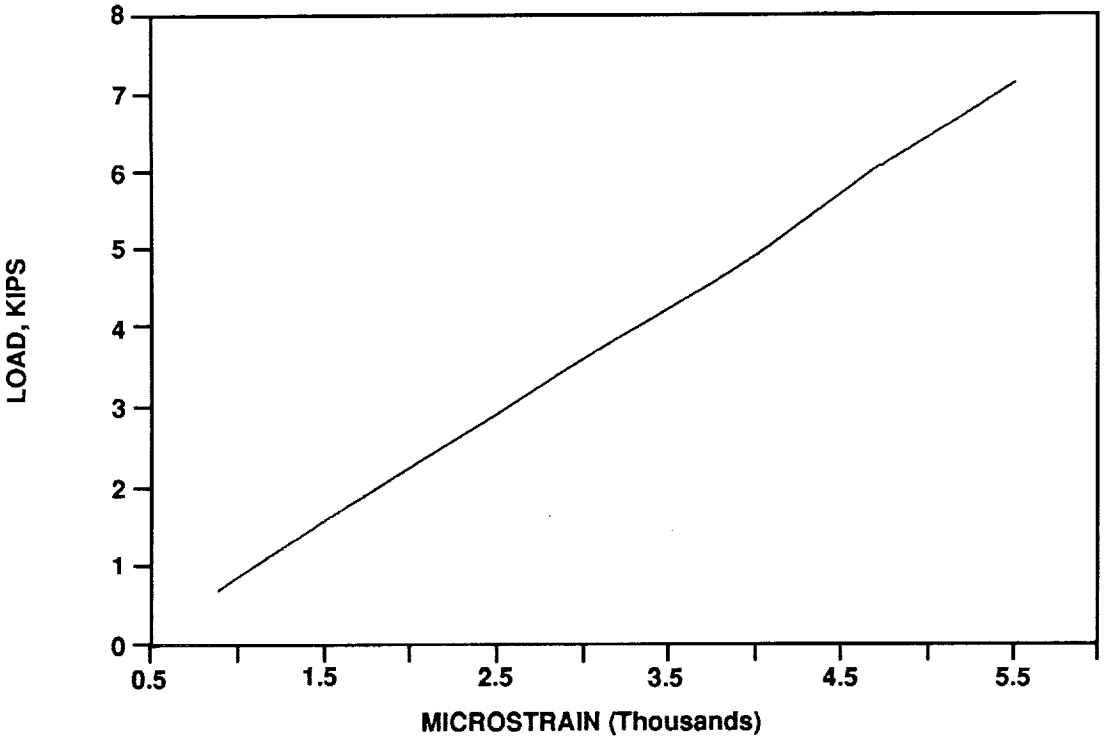

Figure 14. Boot ring beam test No. 3, backup-up 3/9/89, load versus maximum tension strain, specimen No. 1.

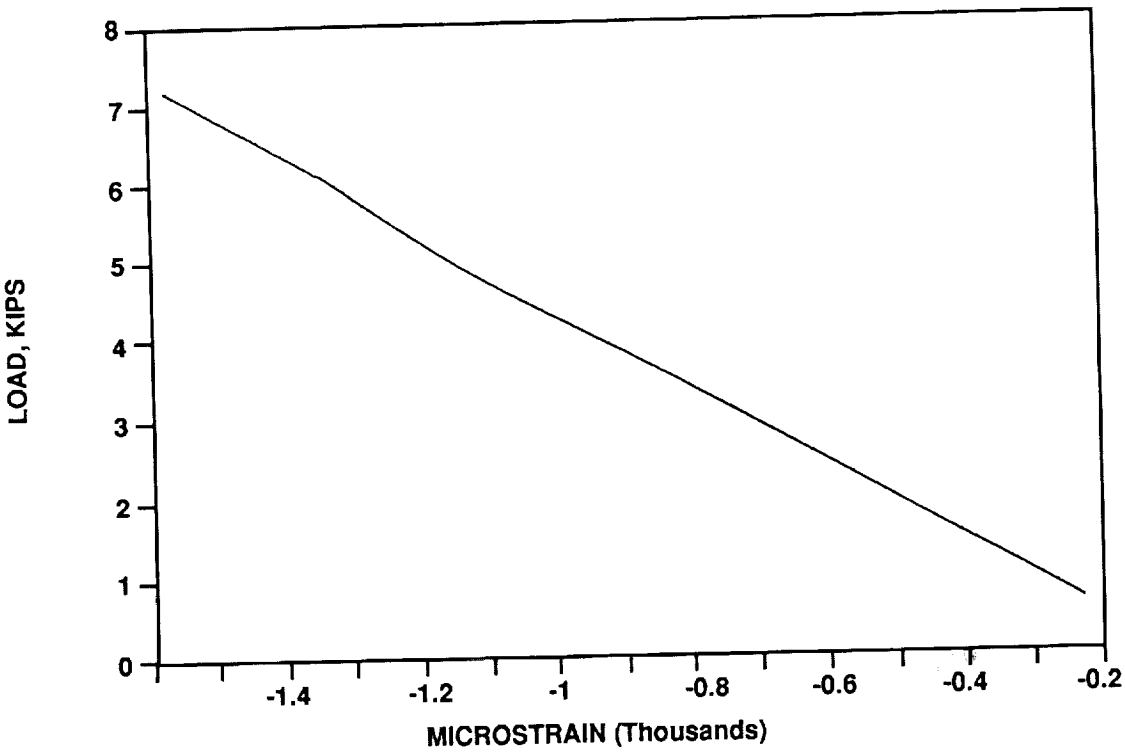

Figure 15. Boot ring beam test No. 3, backup-up 3/9/89, load versus maximum transverse strain, specimen No. 1.

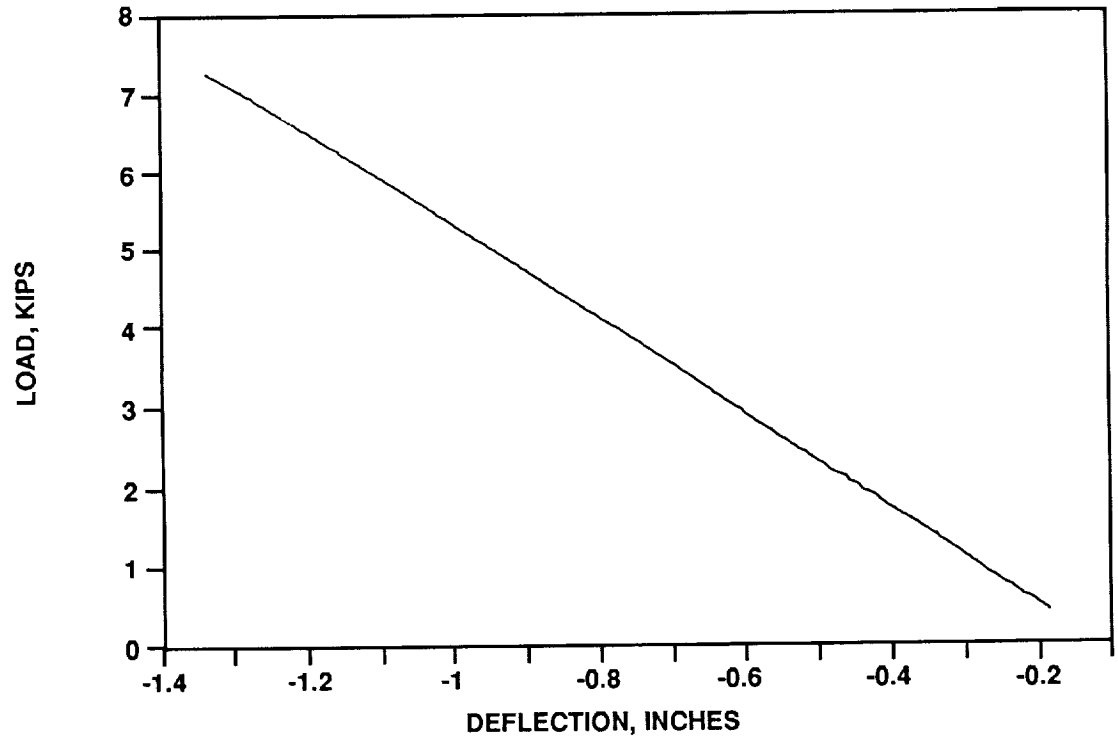

Figure 16. Boot ring beam test No. 1, backup-down 3/9/89, load versus deflection, specimen No. 1.

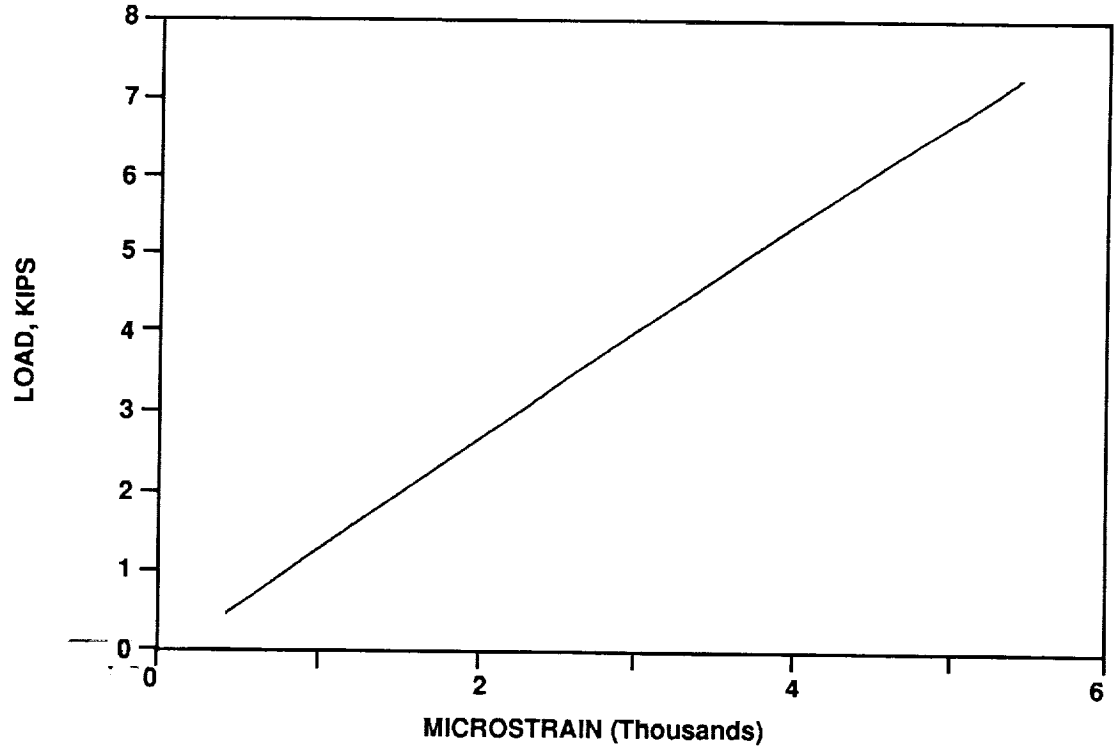

Figure 17. Boot ring beam test No. 1, backup-down 3/9/89, load versus maximum tension strain, specimen No. 1.

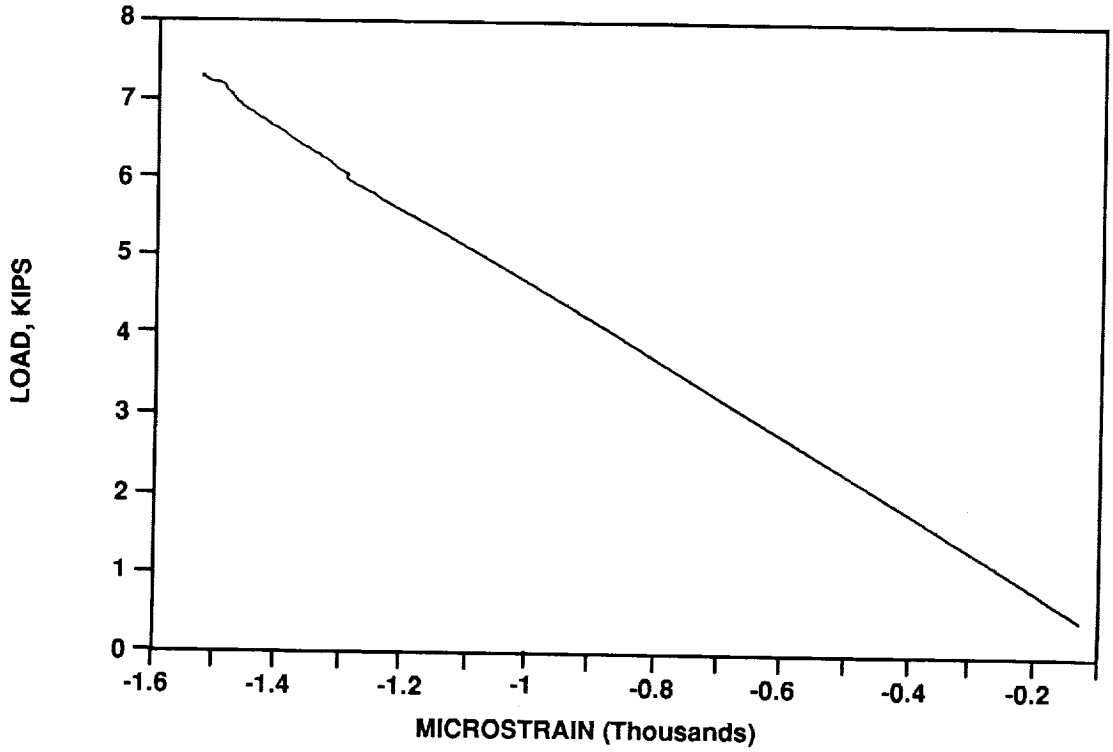

Figure 18. Boot ring beam test No. 1, backup-down 3/9/89, load versus maximum transverse strain, specimen No. 1.

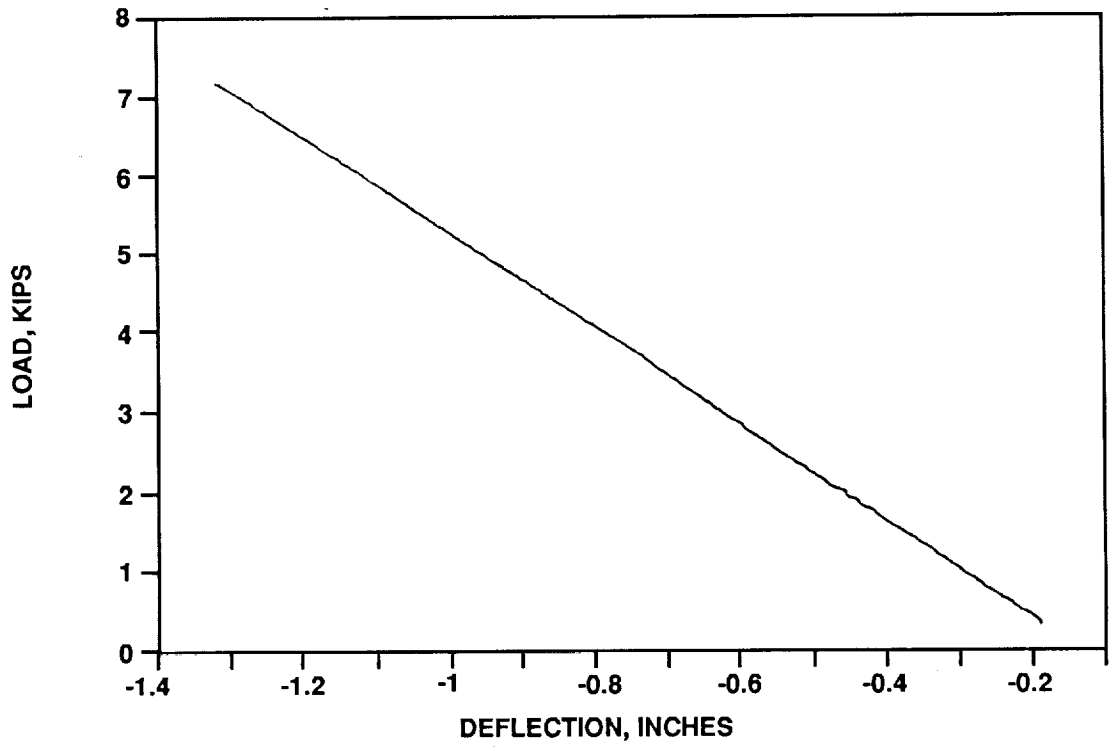

Figure 19. Boot ring beam test No. 2, backup-down 3/9/89, load versus deflection, specimen No. 1.

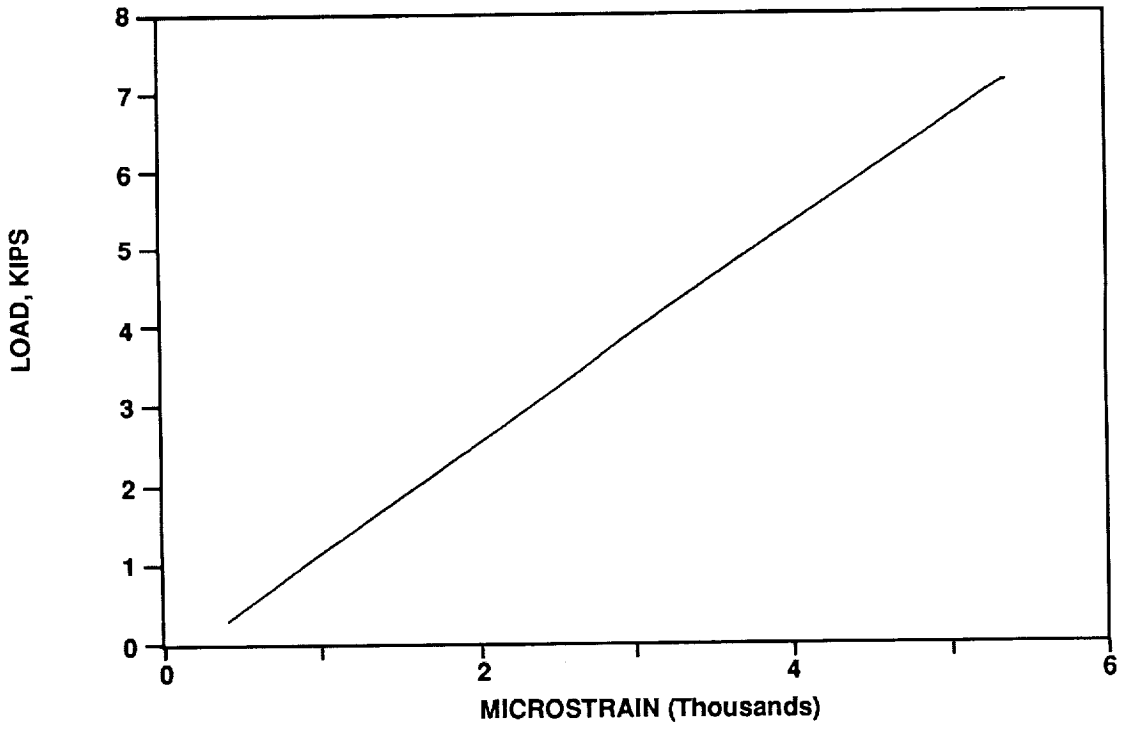

Figure 20. Boot ring beam test No. 2, backup-down 3/9/89, load versus maximum tension strain, specimen No. 1.

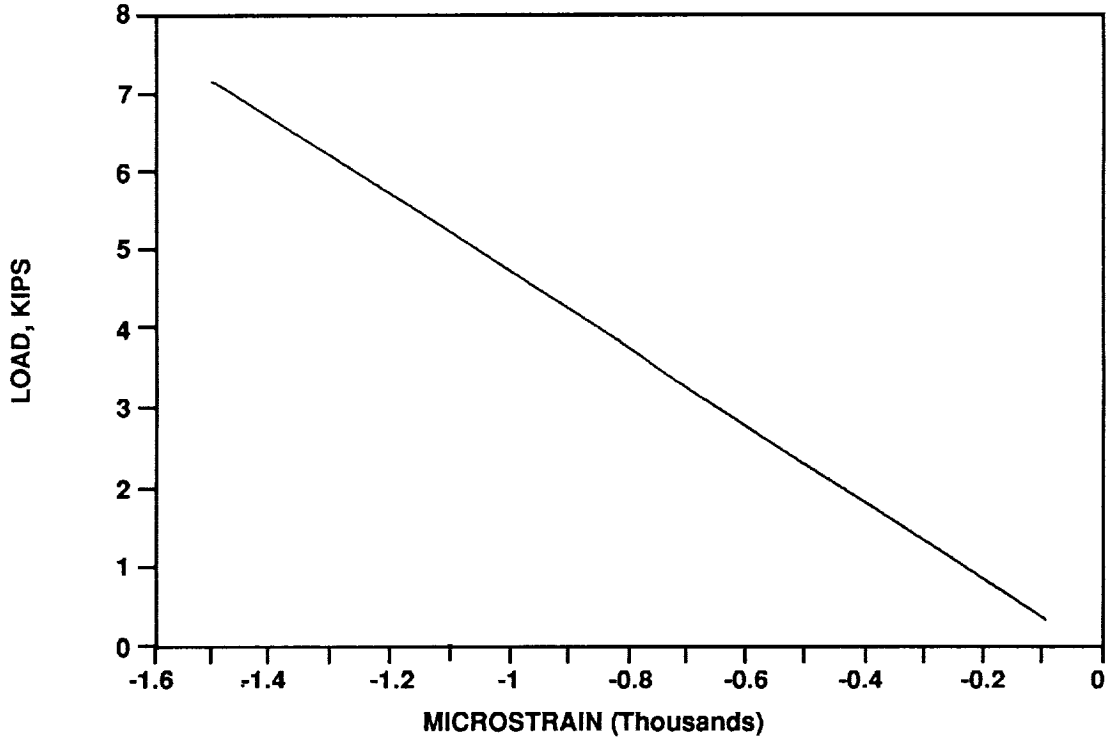

Figure 21. Boot ring beam test No. 2, backup-down 3/9/89, load versus maximum transverse strain, specimen No. 1.

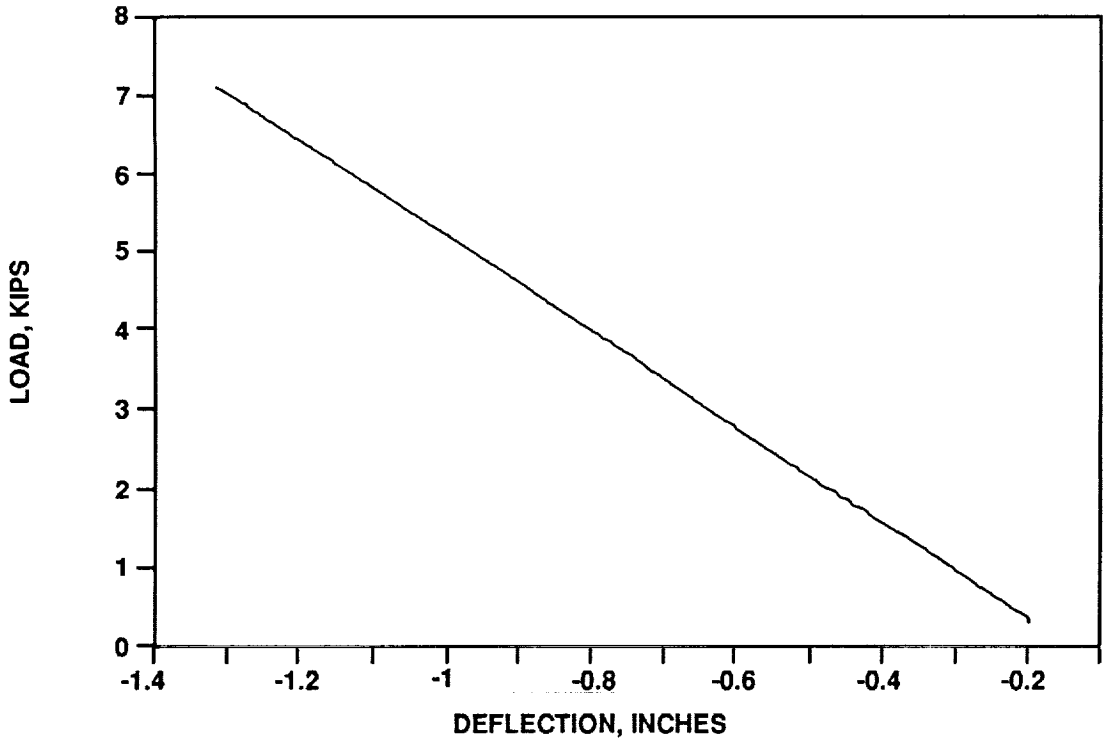

Figure 22. Boot ring beam test No. 3, backup-down 3/9/89, load versus deflection, specimen No. 1.

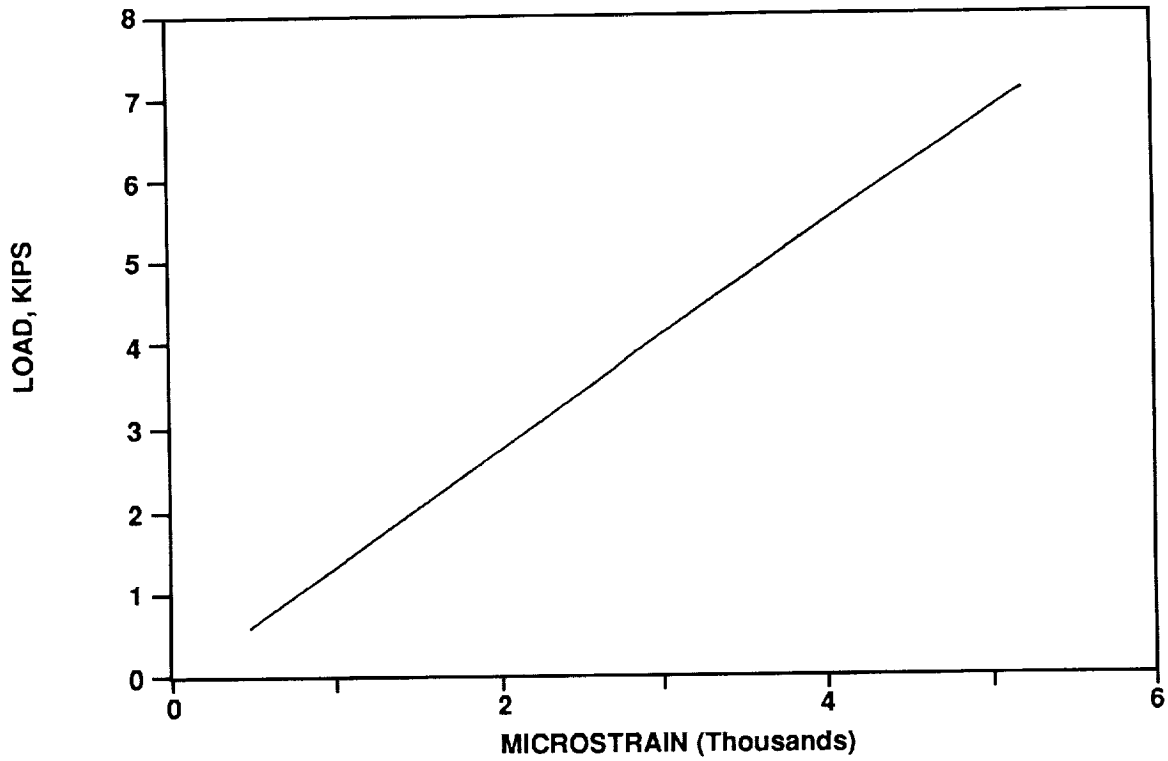

Figure 23. Boot ring beam test No. 3, backup-down 3/9/89, load versus maximum tension strain, specimen No. 1.

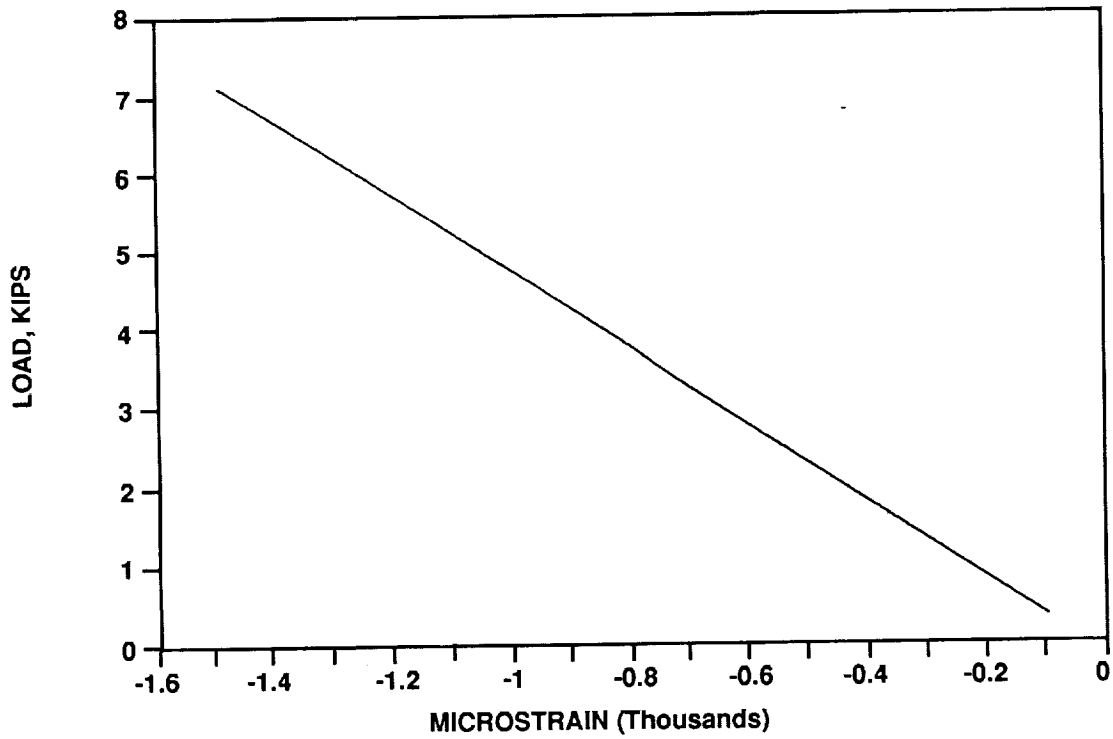

Figure 24. Boot ring beam test No. 3, backup-down 3/9/89, load versus maximum transverse strain, specimen No. 1.

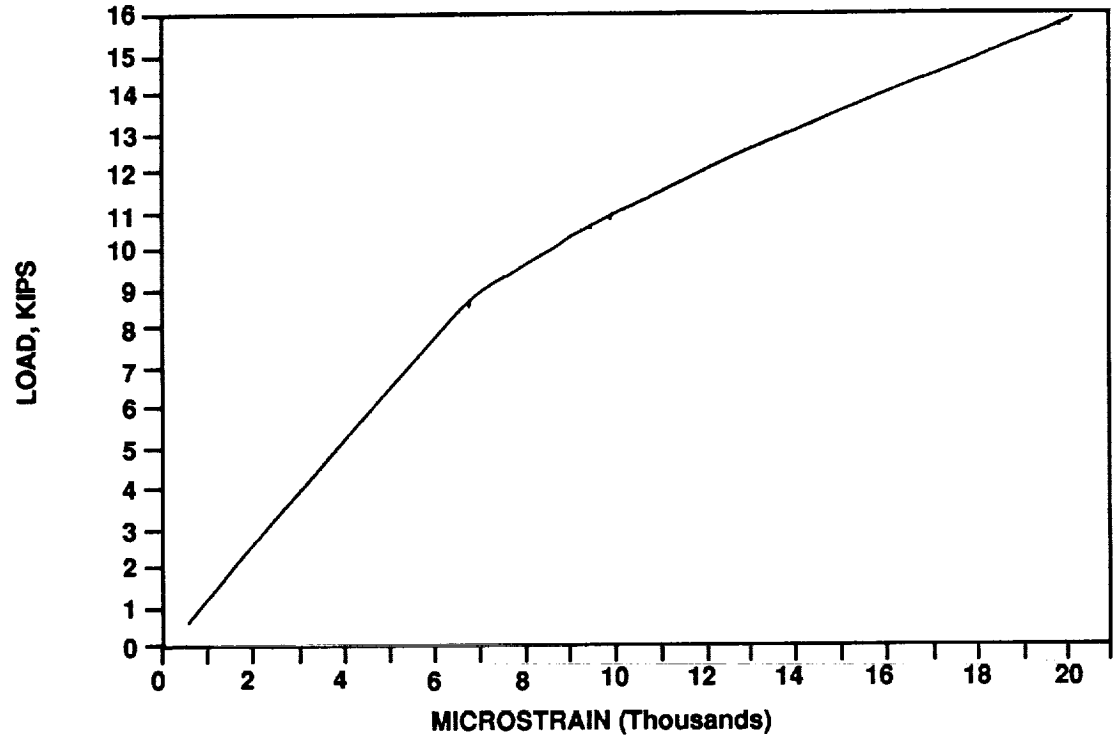

Figure 25. Boot ring beam ultimate test, backup-up 3/9/89, load versus maximum tension strain, specimen No. 1.

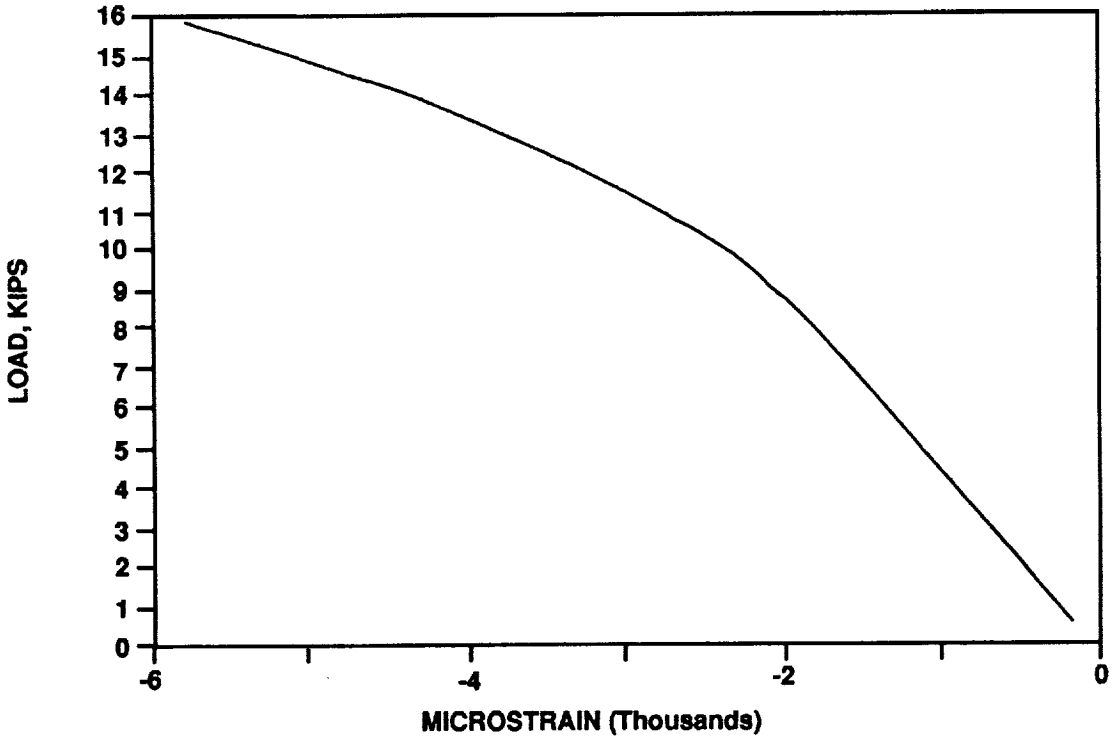

Figure 26. Boot ring beam ultimate test, backup-up 3/9/89, load versus maximum transverse strain, specimen No. 1.

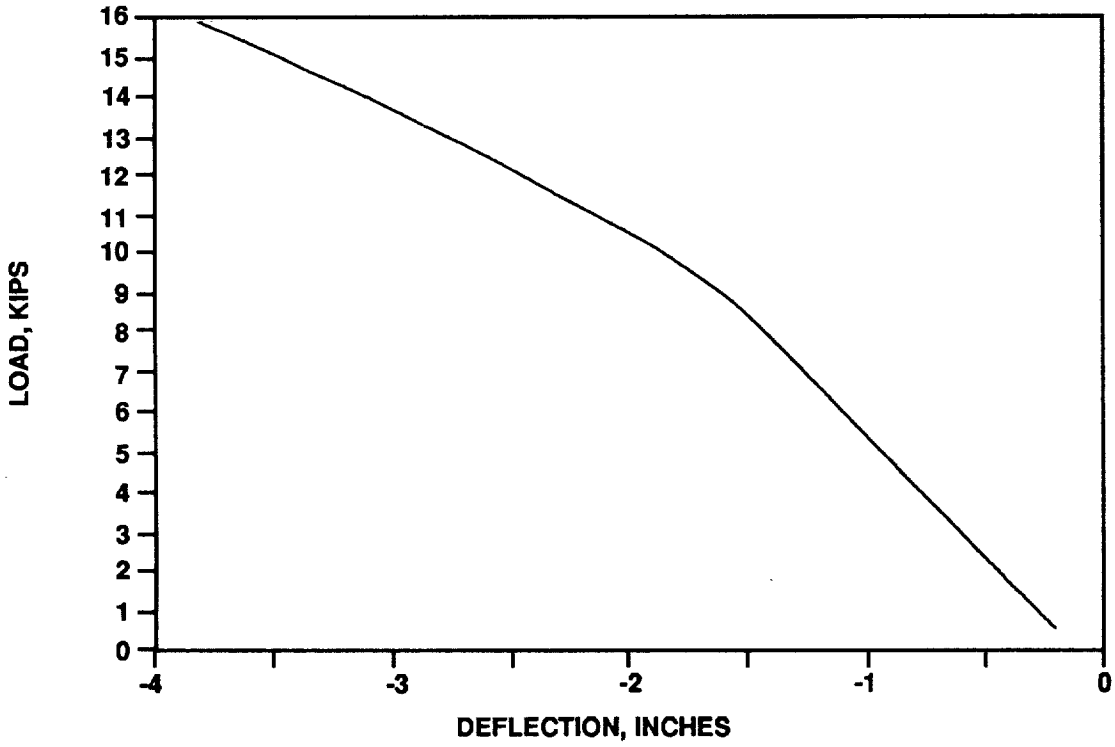

Figure 27. Boot ring beam ultimate test, backup-up 3/9/89, load versus deflection, specimen No. 1.

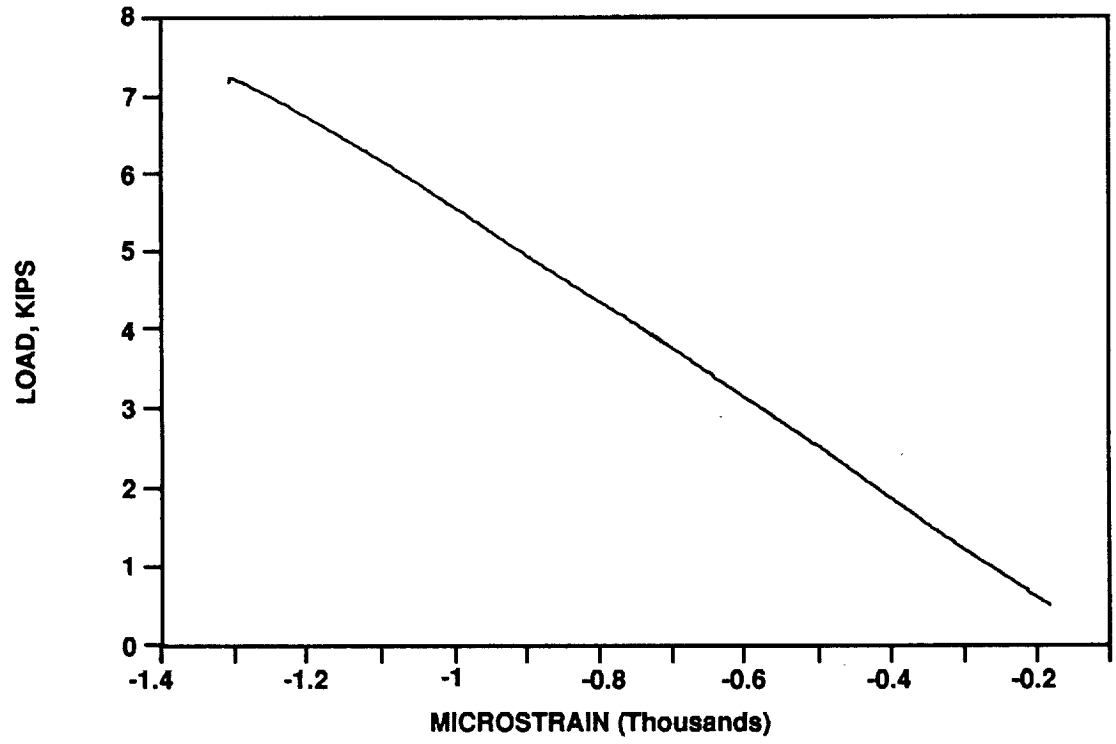

Figure 28. Boot ring beam test No. 1, backup-up 5/10/89, load versus deflection, specimen No. 2.

NASA

Report Documentation Page

1. Report No.	2. Government Accession No.	3. Recipient's Catalog No.
NASA TP-3028		

4. Title and Subtitle

Loads Analysis and Testing of Flight Configuration Solid Rocket Motor Outer Boot Ring Segments

5. Report Date

June 1990

6. Performing Organization Code

7. Author(s)

Rafiq Ahmed

8. Performing Organization Report No.

10. Work Unit No.

M-634

9. Performing Organization Name and Address

George C. Marshall Space Flight Center
Marshall Space Flight Center, AL 35812

11. Contract or Grant No.

13. Type of Report and Period Covered

Technical Paper

12. Sponsoring Agency Name and Address

National Aeronautics and Space Administration
Washington, D.C. 20546

14. Sponsoring Agency Code

15. Supplementary Notes

Prepared by Structures and Dynamics Laboratory, Science and Engineering Directorate.

16. Abstract

This report details the loads testing on in-house-fabricated flight configuration SRM outer boot ring segments. The tests determined the bending strength and bending stiffness of these beams and showed that they compared well with the hand analysis. The bending stiffness test results compared very well with the finite element data.

17. Key Words (Suggested by Author(s))	18. Distribution Statement
Composite Materials, Carbon Phenolic Materials, Outer Boot Ring, Solid Rocket Motor	Unclassified – Unlimited Subject Category 39

19. Security Classif. (of this report)	20. Security Classif. (of this page)	21. No. of pages	22. Price
Unclassified	Unclassified	48	A03

NASA FORM 1626 OCT 86

For sale by the National Technical Information Service, Springfield, VA 22161-2171